Optimizing Region of Interest Registration for Multiple-Tissue Whole Slide Images

Anonymous, Anonymous, and Anonymous

[1] Anonymous
[2] Anonymous Anonymous
Anonymous
[3] Anonymous
Anonymous

Abstract. Digital pathology transforms clinical workflows by enabling the analysis of whole slide images (WSIs) on computers. While most methods focus on haematoxylin and eosin (H&E) stained WSIs, immunohistochemistry (IHC) is crucial for biomarker analysis, particularly for assessing tumour-infiltrating lymphocyte (TIL) subtypes inside a region of interest (ROI) selected by a pathologist using Salgado's criteria.
This study first investigates the naive approach, which verifies a state-of-the-art WSI registration method's robustness for registering single-tissue H&E and multiple-tissue IHC WSIs. Then, to simplify this first attempt by accomplishing registration between single tissues, the study proposes two approaches: splitting the multiple-tissue IHC WSIs, which is considered the baseline, and a virtualised splitting with an incremental resolution optimization-based technique. ROI registration predictions for TIL assessment will be assessed on IHC WSIs using standard metrics and one derived from a standard landmark-based metric popular in the image registration field. Existing image detection-inspired metrics for evaluating ROI proposals will be proposed and tuned to consider the global viewpoint, where the ROI proposals lie.
This study aims to establish a reliable and time-efficient ROI registration procedure for WSIs with multiple stained tissues. This method would enable efficient selection of the ROI from the H&E WSI and potentially reduce the need for pathologist intervention through automatic quality control.

Keywords: Region of interest · Whole slide image · Registration · Multiple tissues · Tumour-infiltrating lymphocyte

1 Introduction

Histological assessment is crucial to the disease's diagnosis, prognosis and treatment phases. As scientific research advances, computational pathology significantly impacts traditional clinical workflows within pathology laboratories [1]. Nowadays, thanks to advances in computer vision in digital pathology, pathologists can analyse digitised slide images, called whole slide images (WSIs), through the aid of computer-assisted pathology (CAP) tools [2].

Currently, most CAP tools focus on analysing WSIs of tissues stained with haematoxylin and eosin (H&E) [3]. However, in the diagnostic workflow, tissues stained with immunohistochemistry (IHC) are also analysed as they allow the scoring of specific biomarkers. Given these two types of staining, it is possible to unlock new fields of research and clinical applications by integrating information between several differently stained tissues [1].

This combination of information from multiple WSIs may be spatially registered to be combined at the tissue level, and the WSI registration technique aids in doing this [1]. This registration process is challenging as different technical factors come into play, mainly the manipulation of gigapixel-scale data, changes in the structure and shape of the other stained tissues, and the presence of artefacts and tears due to the tissue preparation phase [1].

Thus, WSI registration of slides with different staining techniques helps identify patterns and spatial relations within a given specimen [1].

Indeed, this WSI registration process is helpful for an in-depth assessment of tumour-infiltrating lymphocytes (TILs), as it is not possible to know the positiveness of specific biomarkers for these lymphocytes, which may promote tumour progression or inhibit it, by using H&E WSIs alone [4]. Therefore, pathologists, to have a comprehensive landscape of the immune environment for breast cancer (BC), should not only take into account the evaluation of TILs but also the patterns and spatial relationships of immune cells related to the world of TILs, such as macrophages CD163+ and T lymphocytes CD8+ [5, 6].

This spatial alignment of cuts with different stains may help recognise a specific area called the region of interest (ROI) between various cuts, which is the area where TILs are assessed. It begins with the pathologist, who identifies the ROI for assessing TILs in the WSI of the H&E-stained tissue through Salgado's criteria [4]. Once this is done, using the WSI registration process, the exact ROI is automatically found in the remaining sections stained with IHC procedures to recognise the different biomarkers. By doing that, pathologists can make assessments of biomarkers at the spatial level and within the ROI, providing additional insights into the biomarkers's distribution.

However, artefacts, tears, and additional tissues within the WSIs can complicate this registration process. As mentioned earlier, artefacts can be introduced during tissue processing, cutting, staining (e.g., pen marks, ink, tissue folds, dust, air bubbles), or during the scanning phase (e.g., out-of-focus areas of the WSIs) [7–9]. Multiple tissues on a single slide are not considered artefacts since they are an intentional practice to reduce procedural costs. This choice is made during the tissue preparation phase rather than a mistake or oversight in the procedure.

Once the challenges of WSI registration between different stains and the issue of multiple tissues in the same WSI have been introduced, the first aim of this work is to test the robustness of a state-of-the-art (SOTA) procedure for registration under these complexities. The choice of the SOTA technique fell on the Virtual Alignment of pathoLogy Image Series (VALIS) method [10] as it is not only one of the best WSI registration algorithm proposals in the

ACROBAT challenge [1, 11], but also claims to be stain agnostic, scalable and robust. Therefore, the initial test determines whether VALIS is robust enough to accurately register a pair of H&E and IHC WSIs despite the presence of extra tissues. To assess this test with a more straightforward task for VALIS, this work proposes two approaches to facilitate registration for the VALIS technique. The first approach consists of splitting the multiple-tissue IHC WSI into several single-tissue IHC WSIs, while the second approach splits the IHC WSI, but at a lower resolution and without making WSIs, so a virtual split. The comparison of the three methods for the prediction of ROI will be conducted not only with standard metrics such as Intersection over Union (IoU) and Dice Score but also with a metric derived from relative Target Registration Error (rTRE), introduced in the ANHIR challenge [12], which assesses landmark-based registration error. In addition, metrics derived from the image detection field and then tweaked for this case study will be introduced [13, 14].

By evaluating the naive test on the VALIS and then the two proposed approaches, this work points out if the multiple tissues on the IHC WSIs are a problem for this SOTA technique and if using the two proposed approaches can be mitigated. Thus, the aim is to select the correct tissue from the multiple-tissue IHC WSI, register it with the H&E image, and use it for ROI prediction.

With the introduction of virtual splitting, this work aims to evaluate the possibility of reducing the time-consuming step of splitting multiple-tissue IHC WSIs. This proposed approach also aims to incorporate an automated quality control function, significantly reducing the pathologist's participation to validation when needed.

2 Data collection and preparation

This work was carried out on twenty case studies, each consisting of three WSIs: a WSI of breast cancer tissue stained with H&E, a WSI of breast cancer tissue with one or more lymphatic ganglion tissues stained using the CD163 marker, and a WSI of breast cancer tissue with one or more lymphatic ganglion tissues stained using the CD8 marker. Tissue positions may vary between IHC WSIs of the same specimen. The digitised H&E and IHC stained tissue slides are consecutive.

The tissue slides were digitised at 20× magnification using a PANNORAMIC 250 Flash 3DHistech scanner. To identify and separate the different tissues within each IHC WSI, an expert used QuPath, an open-source platform popular in digital pathology to divide the tissue compartments with lines [15]. This manual annotation was necessary to have a ground truth of the tissue compartments, as they can be provided partially overlapping or with such tears and deformations that can lead to ambiguities in the accurate division of these within the IHC WSI. A pathologist, following Salgado's criteria [4], identified the ROI for evaluating TILs on the H&E image of each specimen. After finding the ROI, the pathologist annotated it using SlideViewer, proprietary software developed by 3DHistech. The ROIs annotated by the expert at the lowest level had a rectangular shape

with dimensions of (4050 px ± 40 px) × (7831 px ± 20 px). ROIs are then converted into GeoJSON format, which is compatible with QuPath.

3 Method

The registration of the ROI from the H&E WSI onto the multiple-tissue IHC WSI is based on the VALIS technique [10], a SOTA method for WSI registration in histological images. However, it is modified to perform only rigid registration, specifically an Euclidean transformation, to preserve the shape of the ROI, as all WSIs have the identical resolution.

Therefore, non-rigid registration should be avoided, as it may alter the structural morphology of the tissue within the ROI, which could then have consequences for the TIL assessment.

In this work, the H&E image is the reference image, while the multiple-tissue IHC WSI is the moving image. It can be seen as an example of a pair of reference and moving images from the same case study in Figure 1. After registration, the coordinates of the ROI vertices are warped from the reference image to the moving image to reconstruct the ROI in the multiple-tissue IHC WSI.

3.1 Approaches

The *Naive* approach, depicted in Figure 2, shows the initial registration test. It carries out the registration phase without preprocessing the H&E WSI as the reference image and the multiple-tissue IHC WSI as a moving image. By conducting this trial, it is possible to test the robustness of VALIS in registering the pair of WSIs even in the presence of extra tissue, providing so an additional challenge to it.

To simplify the task, this work introduces the following approach, *Baseline*, depicted in Figure 3. This method aims to facilitate the registration task by adapting it to the case study of the ACROBAT challenge. The approach splits the multiple-tissue IHC WSIs into different single-tissue IHC WSIs to make this fit. To determine which single-tissue IHC WSIs are the ones with breast cancer tissue, the registration that minimises the median rTRE (mrTRE) of the features extracted from VALIS using Binary Robust Invariant Scalable Keypoints (BRISK) [16] and Oxford Visual Geometry Group (VGG) descriptor [17] is selected. These features are matched using brute force, with outliers removed using the Random Sample Consensus (RANSAC) algorithm [18].

However, physically adapting the original data to avoid the problem of extra tissue consumes a lot of time. This issue is because the single-tissue WSIs to be artificially created are of giga-pixel scale size, and different checks have to be performed compared to the compartmentalisation annotations previously carried out by experts.

To optimize this initial step, this work proposes the ***V****irtual* ***S****plitting with* ***I****ncremental* ***R****esolution* ***O****ptimization* (*VSIRO*) approach, as shown in Figure 4. This method uses annotations from experts to identify tissue compartment

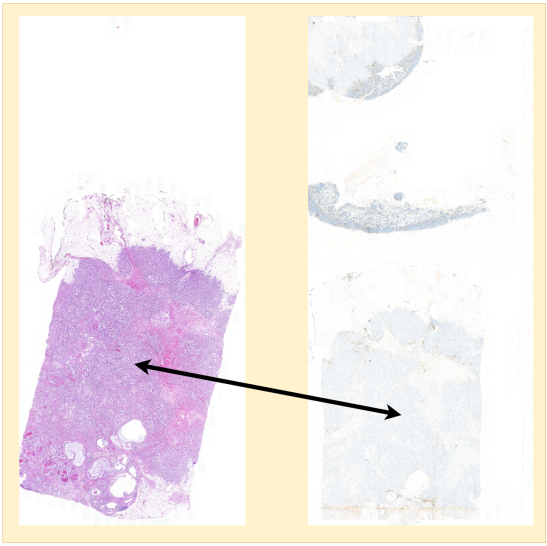

Fig. 1. A pair of WSIs from the same case study can be seen. On the left is the H&E WSI of breast cancer tissue, which is used as the reference image. On the right, it is possible to visualize the multiple-tissue WSI with IHC staining for CD8 biomarker where at the top is tissue from a positive non-sentinel ganglion, in the middle is tissue from a negative non-sentinel ganglion, and at the bottom is breast cancer tissue. The multiple-tissue IHC WSI is used as the moving image. The arrow shows the correspondence between the tissue in the H&E WSI and the breast cancer tissue in the multiple-tissue IHC WSI.

areas in each multiple-tissue IHC WSI. It then creates multiple masks at a higher level for the multiple-tissue IHC WSIs.

Thus, the method selects the same level for both WSIs since they share the exact resolution and number of levels. If there were differences in resolution or levels between the pair of WSIs, it may turn to similarity transformation registration.

This approach allows VALIS to work with smaller images at lower resolution levels, speeding up the process.

However, attention must be paid to the dimension of the images as if they are too small; there is a risk of losing too much information to give in input to the registration phase. Therefore, the $VSIRO$ approach extracts the multiple-tissue IHC image from the highest available level (level t) where the image width is larger but, at the same time, closer to the resize threshold than the VALIS width (850 px). After splitting the multiple-tissue image into n flat images containing a single tissue, $VSIRO$ performs n registrations with the reference H&E image at the same level as each single-tissue IHC image.

VSIRO approaches compute the ratio between the second-lowest mrTRE and the lowest mrTRE among the n registrations. If this ratio exceeds a threshold r (set to 2), the second-lowest mrTRE is at least twice the lowest mrTRE, suggesting a reliable registration. If the ratio is less than r, it implies uncertainty in correctly identifying the tissue for registration.

The procedure is repeated using the next lower level of the multiple-tissue IHC image to reach a more confident tissue selection. Registration is considered unreliable if it gets the minimum extractable level (*minLevel*) of the multiple-tissue IHC WSI without obtaining a reliable result (the ratio exceeds r). Hardware limitations may also set this *minLevel*.

Suppose a reliable result is achieved. In that case, it warps the ROI of the reference image using the registration parameters of the IHC tissue with the lowest mrTRE among the n images.

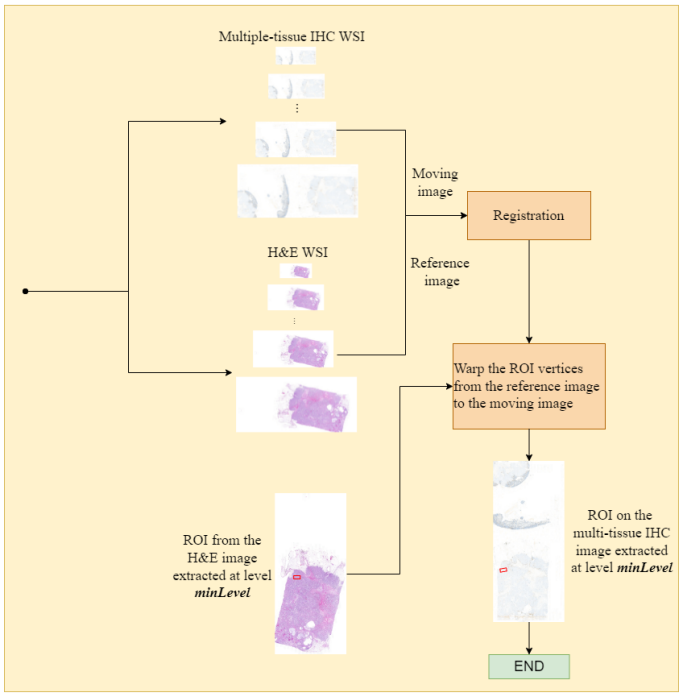

Fig. 2. Diagram illustrating the *Naive* approach for ROI registration. In this method, the H&E WSI is used as the reference image, and the multiple-tissue IHC WSI is the moving image.

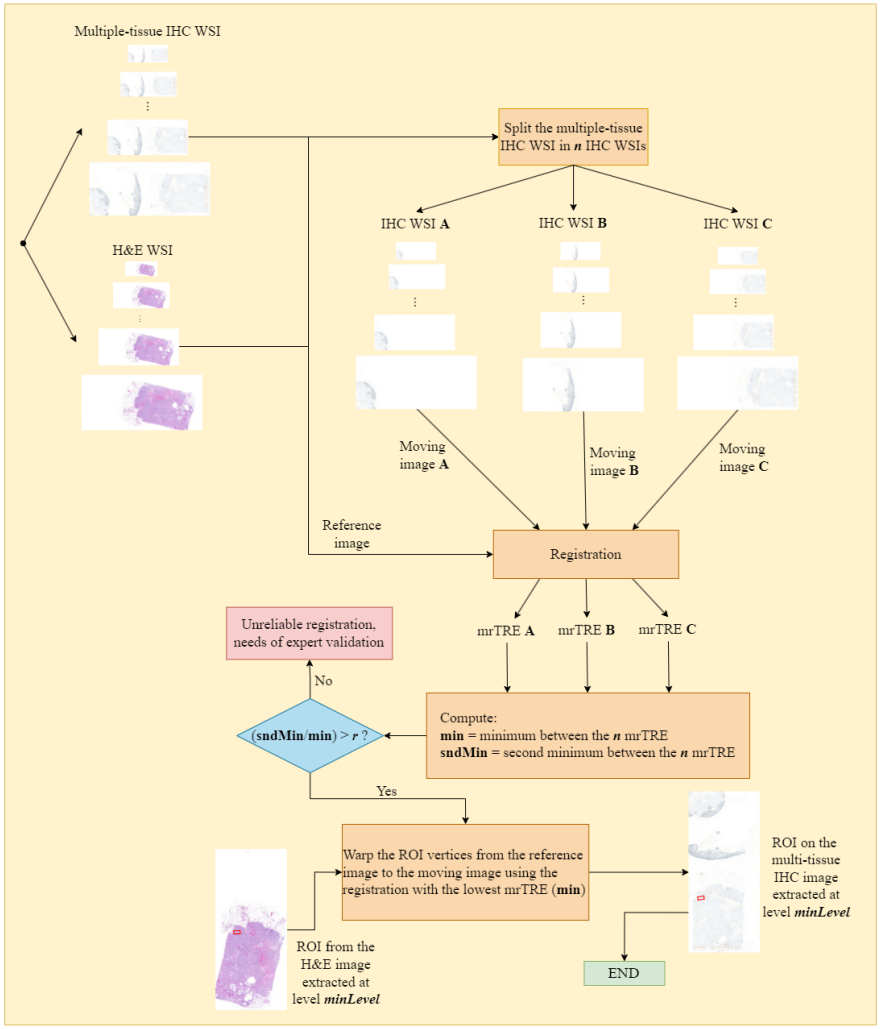

Fig. 3. Diagram depicting the *Baseline* method for ROI registration. The multiple-tissue IHC WSI is split into single-tissue IHC WSIs, each containing a single tissue type. Registration is performed separately on the H&E image using each IHC WSI. Subsequently, the ROI is determined using the registration parameters from the IHC WSI with the lowest mrTRE.

3.2 Metrics

To evaluate the three approaches and their likeness, this work first employs the popular IoU and Dice Score, which are adapted slightly for the case study (Equation 1 and Equation 2):

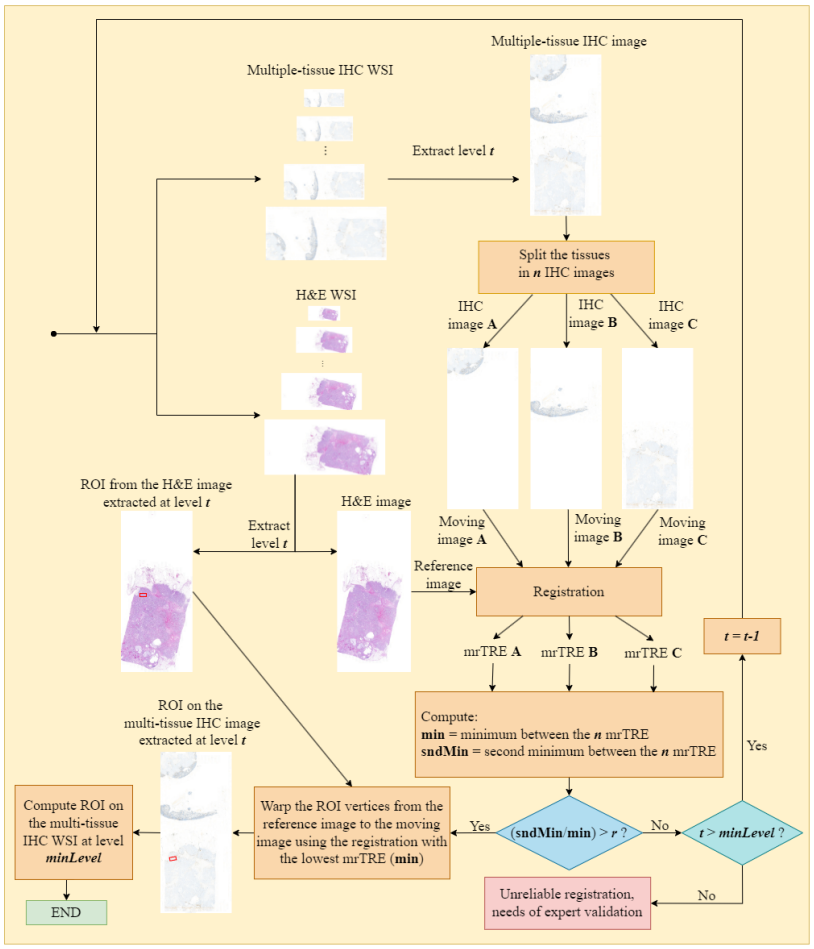

Fig. 4. Diagram illustrating the *VSIRO* approach for ROI registration. The multiple-tissue IHC WSIs are virtually separated at a higher level to extract smaller image compartments. Registration is then applied to these tissues using the corresponding H&E image extracted at the same level. The registration parameters chosen are from the IHC image with the lowest mrTRE. Quality control checks ensure accurate tissue selection; if discrepancies arise, it restarts by extracting the following lower-level images of both WSIs.

$$IoU_l^{ij} = \frac{|R_l^i \cap R_l^j|}{|R_l^i \cup R_l^j|} \tag{1}$$

$$DiceScore_l^{ij} = \frac{|2 \times (R_l^i \cap R_l^j)|}{|R_l^i| + |R_l^j|} \tag{2}$$

where R_l^i is the ROI proposal using the approach i on the WSI l, and R_l^j of the approach j on the WSI l.

Additional metrics are then incorporated. First, it is introduced a metric called rTRE of the centroids (rTREc), presented in Equation 3, which computes the rTRE between the centroids of paired ROIs from two compared approaches:

$$rTREc_l^{ij} = \frac{\|c_l^i - c_l^j\|_2}{d_l} \tag{3}$$

where c_l^i is defined as the centroid of the ROI of the WSI l computed using the approach i, c_j^i of the approach j and d_l is the length of the diagonal image l.

Next, it is redefined the Generalized IoU (GIoU) [13] and Distance IoU (DIoU) [14] metrics for this case study, respectively defined in Equation 4 and Equation 5, inspired from the bounding boxes used in image detection, as the ROIs are rectangular:

$$GIoU_l^{ij} = IoU_l^{ij} - \frac{|S_l^{ij} \setminus (R_l^i \cup R_l^j)|}{|S_l^{ij}|} \tag{4}$$

$$DIoU_l^{ij} = IoU_l^{ij} - \frac{\|c_l^i - c_l^j\|_2}{d^2_{S_l^{ij}}} \tag{5}$$

where S_l^{ij} is the smallest rectangle enclosing R_l^i and R_l^j in the image l. [13] suggests that S_l^{ij} can be a rectangle since it can have the same convex shape type as the enclosed shapes. After that, $d^2_{S_l^{ij}}$ is the length square of the diagonal of the S_l^{ij} rectangle.

Finally, these new metrics are proposed: Global GIoU (GGIoU) and Global GDIoU (GDIoU), respectively defined in Equation 6 and Equation 7, which take into consideration also the dimension of the entire image. The first one, as it can be seen from the derived name, takes inspiration from GIoU, while the latter takes from DIoU by doing a normalisation inspired from the rTRE metric:

$$GGIoU_l^{ij} = IoU_l^{ij} - \frac{|S_l^{ij} \setminus (R_l^i \cup R_l^j)|}{|l|} \tag{6}$$

$$GDIoU_l^{ij} = IoU_l^{ij} - \frac{\|c_l^i - c_l^j\|_2}{d_l} \tag{7}$$

4 Results

The following section presents the registration results by comparing the three approaches pairwise. This work provides two tables for each pair of biomarkers. The first table types (Table 1 and Table 3) show IoU, Dice Score, and rTREc outcomes, which are metrics close to the image registration field [12], while the other two tables (Table 2 and Table 4) propose outcomes metrics adapted for the case study, inspired by bounding boxes used in image detection.

Regarding the number of cycles for the $VSIRO$ approach, it takes 1.1 ± 0.144 cycles for CD163 and 1.2 ± 0.244 cycles for CD8. This outcome implies that in most cases, it only requires the images from the initial chosen level t, demonstrating the efficacy of the $VSIRO$ approach.

Approaches compared	**IoU(↑)**	**DiceScore(↑)**	**rTREc(↓)**
{*Naive*, *Baseline*}	0.461 ± 0.177	0.531 ± 0.192	0.093 ± 0.082
{*Naive*, $VSIRO$}	0.468 ± 0.181	0.534 ± 0.194	0.091 ± 0.082
{*Baseline*, $VSIRO$}	0.674 ± 0.137	0.756 ± 0.140	0.01 ± 0.009

Table 1. Approaches comparison for ROIs predicted on multiple-tissue CD163 WSIs from the H&E WSIs. Approaches are compared pairwise using IoU, Dice Score, and rTREc.

Approaches compared	**GIoU(↑)**	**DIoU(↑)**	**GGIoU(↑)**	**GDIoU(↑)**
{*Naive*, *Baseline*}	0.163 ± 0.350	0.461 ± 0.177	0.453 ± 0.182	0.368 ± 0.239
{*Naive*, $VSIRO$}	0.184 ± 0.344	0.468 ± 0.181	0.459 ± 0.186	0.377 ± 0.242
{*Baseline*, $VSIRO$}	0.582 ± 0.225	0.674 ± 0.137	0.674 ± 0.138	0.664 ± 0.146

Table 2. Approaches comparison for ROIs predicted on multiple-tissue CD163 WSIs from the H&E WSIs. Approaches are compared pairwise using GIoU, DIoU, GGIoU, and GDIoU.

5 Discussion

The *Naive* approach, which tries to register without preprocessing the H&E WSI with the multiple-tissue IHC WSI, cannot be used for this case study. This issue is because the task is too tricky for VALIS and is based only on its rigid registration phase. Therefore, the *Baseline* approach is recommended as a starting point, leading back to a more straightforward case study, so registration between single tissues with different stains.

From an overall standpoint, the results between CD163 and CD8 are similar. These outcomes are due since they are biomarkers with the same colour stain from equal specimens, prepared from the same lab and digitised with the same WSI scanner [5]. The comparisons between the *Naive* method and the *Baseline*

Approaches compared	**IoU(↑)**	**DiceScore(↑)**	**rTREc(↓)**
{*Naive*, *Baseline*}	0.495 ± 0.187	0.553 ± 0.201	0.082 ± 0.067
{*Naive*, *VSIRO*}	0.497 ± 0.189	0.554 ± 0.202	0.062 ± 0.043
{*Baseline*, *VSIRO*}	0.650 ± 0.135	0.742 ± 0.131	0.034 ± 0.059

Table 3. Approaches comparison for ROIs predicted on multiple-tissue CD8 WSIs from the H&E WSIs. Approaches are compared pairwise using IoU, Dice Score, and rTREc.

Approaches compared	**GIoU(↑)**	**DIoU(↑)**	**GGIoU(↑)**	**GDIoU(↑)**
{*Naive*, *Baseline*}	0.191 ± 0.367	0.495 ± 0.187	0.486 ± 0.192	0.413 ± 0.240
{*Naive*, *VSIRO*}	0.197 ± 0.366	0.497 ± 0.189	0.491 ± 0.193	0.435 ± 0.226
{*Baseline*, *VSIRO*}	0.548 ± 0.221	0.650 ± 0.135	0.647 ± 0.138	0.616 ± 0.176

Table 4. Approaches comparison for ROIs predicted on multiple-tissue CD8 WSIs from the H&E WSIs. Approaches are compared pairwise using GIoU, DIoU, GGIoU, and GDIoU.

or *VSIRO* methods show a divergence in both approaches since ROI prediction using the *Naive* method requires intervention in 6/20 CD163 and 7/20 CD8 biomarker cases.

As can be noticed, there is a strong relation between the *Baseline* and *VSIRO* methods for both biomarkers. The failures encountered with CD163 occurred on two case studies with the *Baseline* method, which, even though it had chosen the correct single-tissue IHC WSI, could have been more successful in registering ROIs. For the CD8 biomarker, the quality control detected a failure in tissue selection on a case study with the *VSIRO* approach, which selected the wrong tissue. In this case, the ratio between the first and second minimum rTRE values did not pass the threshold r (ratio = 1.776), necessitating pathologist intervention. Note that even in the *Baseline* approach, it did not pass the r (ratio = 1.097) for the same case study. Therefore, it did not pass the quality control, but *Baseline* however took the correct tissue for the ROI. Based on a *VSIRO* split, this approach eliminates the need to physically split the multiple-tissue WSIs, providing a more time-efficient solution.

Baseline and *VSIRO* workflows significantly reduce the need for pathologist intervention, limiting it to only the most complex cases, when the quality control phase detects uncertainty in tissue selection.

The proposed metrics, GGIoU and GDIoU, are intended to enlarge the viewpoint of GIoU and DIoU metrics, which mainly focus on the local area comprising the two ROI proposals. The proposed metrics, GGIoU and GDIoU, consider the

image size in which the ROI proposals lie. Unlike GIoU, the GGIoU metric is designed to minimise over-penalisation. In contrast, DIoU provides limited information because its penalty term is too minimal, as it proposes in the denominator the square length of the diagonal of the smallest rectangle surrounding the two ROIs.

6 Conclusion and Future Work

This work aimed to present the ROI registration case study between single-tissue WSIs and multiple-tissue WSIs. After the initial attempt to use a naive SOTA algorithm for WSI registration, this work found it not robust for this case study. The problem should be eased by returning to the single-tissue registration strategy to facilitate this task. However, using the *Baseline* approach by dividing the multiple-tissue WSIs into different single-tissue WSIs consumes too much time. Therefore, the $VSIRO$ approach was presented to split the various tissue compartments without physically dividing them into WSIs. In this way, it is more time-efficient and more valuable in the clinical workflow. In addition, this work introduced a quality control assessment in both *Baseline* and $VSIRO$ approaches to determine whether the methods are confident in computing the ROI prediction in the correct selected tissue. Furthermore, the $VSIRO$ approach uses an incremental strategy that uses higher resolution images only if a smaller image size fails to pass the quality control phase.

Future work will automate the entire pipeline, including automatically splitting the initial compartments without the experts' annotations. This will lead to a fully automatic end-to-end registration process, with pathologist intervention only in complex cases, such as when the quality control phase detects a possible failure.

References

1. Weitz, P., Valkonen, M., Solorzano, L., Carr, C., Kartasalo, K., Boissin, C., Koivukoski, S., Kuusela, A., Rasic, D., Feng, Y., et al.: The ACROBAT 2022 challenge: automatic registration of breast cancer tissue. arXiv preprint arXiv:2305.18033 (2023)
2. Nam, S., Chong, Y., Jung, C.K., Kwak, T.Y., Lee, J.Y., Park, J., Rho, M.J., Go, H.: Introduction to digital pathology and computer-aided pathology. Journal of pathology and translational medicine **54**(2), 125 (2020)
3. Baxi, V., Edwards, R., Montalto, M., Saha, S.: Digital pathology and artificial intelligence in translational medicine and clinical practice. Modern Pathology **35**(1), 23–32 (2022)
4. Salgado, R., Denkert, C., Demaria, S., Sirtaine, N., Klauschen, F., Pruneri, G., Wienert, S., Van den Eynden, G., Baehner, F.L., Pénault-Llorca, F., et al.: The evaluation of tumor-infiltrating lymphocytes (TILs) in breast cancer: recommendations by an International TILs Working Group 2014. Annals of oncology **26**(2), 259–271 (2015)

5. Fortis, S.P., Sofopoulos, M., Sotiriadou, N.N., Haritos, C., Vaxevanis, C.K., Anastasopoulou, E.A., Janssen, N., Arnogiannaki, N., Ardavanis, A., Pawelec, G., et al.: Differential intratumoral distributions of CD8 and CD163 immune cells as prognostic biomarkers in breast cancer. Journal for immunotherapy of cancer **5**, 1–12 (2017)
6. Fiorin, A., López Pablo, C., Lejeune, M., Hamza Siraj, A., Della Mea, V.: Enhancing AI Research for Breast Cancer: A Comprehensive Review of Tumor-Infiltrating Lymphocyte Datasets. Journal of Imaging Informatics in Medicine pp. 1–13 (2024)
7. Smit, G., Ciompi, F., Cigéhn, M., Bodén, A., Van Der Laak, J., Mercan, C.: Quality control of whole-slide images through multi-class semantic segmentation of artifacts. In: Medical Imaging with Deep Learning (2021)
8. Schömig-Markiefka, B., Pryalukhin, A., Hulla, W., Bychkov, A., Fukuoka, J., Madabhushi, A., Achter, V., Nieroda, L., Büttner, R., Quaas, A., et al.: Quality control stress test for deep learning-based diagnostic model in digital pathology. Modern Pathology **34**(12), 2098–2108 (2021)
9. Schreiber, B., Denholm, J., Jaeckle, F., Arends, M.J., Branson, K., Schönlieb, C.B., Soilleux, E.: Rapid artefact removal and H&E-stained tissue segmentation. Scientific Reports **14**(1), 309 (2024)
10. Gatenbee, C.D., Baker, A.M., Prabhakaran, S., Swinyard, O., Slebos, R.J., Mandal, G., Mulholland, E., Andor, N., Marusyk, A., Leedham, S., et al.: Virtual alignment of pathology image series for multi-gigapixel whole slide images. Nature communications **14**(1), 4502 (2023)
11. Weitz, P., Valkonen, M., Solorzano, L., Carr, C., Kartasalo, K., Boissin, C., Koivukoski, S., Kuusela, A., Rasic, D., Feng, Y., et al.: ACROBAT–a multi-stain breast cancer histological whole-slide-image data set from routine diagnostics for computational pathology. arXiv preprint arXiv:2211.13621 (2022)
12. Borovec, J., Kybic, J., Arganda-Carreras, I., Sorokin, D.V., Bueno, G., Khvostikov, A.V., Bakas, S., Eric, I., Chang, C., Heldmann, S., et al.: ANHIR: automatic non-rigid histological image registration challenge. IEEE transactions on medical imaging **39**(10), 3042–3052 (2020)
13. Rezatofighi, H., Tsoi, N., Gwak, J., Sadeghian, A., Reid, I., Savarese, S.: Generalized intersection over union: A metric and a loss for bounding box regression. In: Proceedings of the IEEE/CVF conference on computer vision and pattern recognition. pp. 658–666 (2019)
14. Zheng, Z., Wang, P., Liu, W., Li, J., Ye, R., Ren, D.: Distance-IoU loss: Faster and better learning for bounding box regression. In: Proceedings of the AAAI conference on artificial intelligence. vol. 34, pp. 12993–13000 (2020)
15. Bankhead, P., Loughrey, M.B., Fernández, J.A., Dombrowski, Y., McArt, D.G., Dunne, P.D., McQuaid, S., Gray, R.T., Murray, L.J., Coleman, H.G., et al.: QuPath: Open source software for digital pathology image analysis. Scientific reports **7**(1), 1–7 (2017)
16. Leutenegger, S., Chli, M., Siegwart, R.Y.: Brisk: Binary robust invariant scalable keypoints. In: 2011 International Conference on Computer Vision. pp. 2548–2555 (2011). https://doi.org/10.1109/ICCV.2011.6126542
17. Simonyan, K., Vedaldi, A., Zisserman, A.: Learning local feature descriptors using convex optimisation. IEEE Transactions on Pattern Analysis and Machine Intelligence **36**(8), 1573–1585 (2014). https://doi.org/10.1109/TPAMI.2014.2301163
18. Cantzler, H.: Random sample consensus (ransac). Institute for Perception, Action and Behaviour, Division of Informatics, University of Edinburgh **3** (1981)